Modelling and Control of a Power Flow Controller for DC Microgrids

Tanguy Simon, Jean-François Trégouët, Hervé Morel, Xuefang Lin-Shi

Modelling and Control of a Power Flow Controller for DC Microgrids

Tanguy Simon, Jean-François Trégouët, Hervé Morel and Xuefang Lin-Shi
Univ Lyon, INSA Lyon, Université Claude Bernard Lyon 1, Ecole Centrale de Lyon, CNRS, Ampère, UMR5505
25 avenue Jean Capelle,
69621 Villeurbanne, France
Email: tanguy.simon@insa-lyon.fr

Keywords

≪Power flow control≫,≪Microgrid≫, ≪Modelling≫, ≪Robust control≫, ≪Converter control≫.

Abstract

This paper presents a state feedback control method for a power flow controller for meshed DC micro-grids. A modular generic dynamic model of the system is proposed. This model is augmented with integrators and linearised, and a state feedback control law is proposed to define the duty cycles for the PWM switching of the IGBTs. The power in each line and the voltage of a reservoir capacitor in the converter are directly controlled. The validity of the proposed model and control law are assessed on an experimental setup.

Introduction

Micro-grids are currently being studied as a solution to meet the challenge of reducing the environmental impact of our energy systems. Among the considered applications are buildings and districts, factories and residential or rural areas. One of their global advantages is their ability to increase the penetration of small renewable energy generators [1]. For rural and residential applications, the development of micro-grids increase the independence and empowerment of (energy) communities [2], raise awareness about ones energy consumption and greatly help the transition towards a more energy-frugal lifestyle. The experience of "off-griders" shows that the implication of consumers in their energy production leads to their adaptation in lifestyle and demand to meet the intermittency of renewable sources [3]. Similar behaviour can then be expected from "micro-griders", thereby decreasing the need for storage and over-sizing of the power generation capacity.

The use of direct current (DC) in micro-grids brings various advantages: It removes the problem of reactive power and skin effects. If a voltage standard is chosen appropriately [4], it can reduce the number of power converters needed because most AC generators and loads already have a DC link (wind turbines equipped with a maximum power point tracker (MPPT), AC or DC motors drives, Photovoltaics) [5]–[7]. Moreover, the resistive loads such as electric heaters, ovens or water heaters are able to function equally on DC or AC.

Meshed micro-grids are another line of research proposed to enhance the flexibility of the design and reduce the amount of copper needed for the wiring because the current can be split between different paths. It is especially meaningful when generation units and loads are distributed and enables a fast reconfiguration of the network. More detail about meshed structures, the use of DC and other micro-grid aspects can be found in [8].

In this context, the Power Flow Controller (PFC) must be introduced. This multi-terminal DC/DC converter is required in meshed grids to control the power flow at some strategic nodes (Fig. 1a) or at every

node of the micro-grid. It is a useful actuator for a grid control algorithm when some of the other converters or dipoles cannot be remotely driven, as is often the case. The resulting micro-grid is then much more flexible and modular. This type of converter has been widely studied for high voltage grids (HVDC) [9], but very little for low-voltage systems (LVDC). In the former, PFCs are usually only connected to the positive terminals of the different lines (floating) because withstanding the full line voltage would require a very expensive and inefficient converter topology [9]. This problem disappears with LVDC grids, so that a single PFC can not only regulate line voltages but also act as a DC circuit breaker or even as an MPPT [10].

The authors of [11] propose the use of two split-pi converters to achieve power flow control on a 3-terminal node. However, the proposed control method only focuses on one of the two converters, failing to control the full node. Moreover, it does not achieve power flow control but rather voltage control with a limited current output. [12] propose another topology consisting of a modified split-pi with m half-bridge legs connected to the same reservoir (or link) capacitor instead of two (Fig. 1b). In addition to being simpler, this enables power flow control on a multi-terminal node. Although the topology is promising, no dynamic model of the converter is proposed and the study is limited to a two-terminal version, which does not constitute a node. Moreover, the proposed control approach is open-loop and is therefore expected to be fragile with respect to the uncertainty of the grid. Finally, the reservoir voltage has to be maintained by an additional branch that compensates the transient power imbalance. In [13], a new control law is proposed to improve the power flow control during fluctuations of the reservoir voltage. Unfortunately, the controller regulates the current rather than the power, and the computation of the current reference requires the knowledge of non local information, that is the voltage at the ending of the line. For these reasons, a fluctuation in the loads or generation units of the grid would lead to a steady-state error of the power. Furthermore, the reservoir voltage remains uncontrolled and there is therefore no guarantee that it will remain within the physical boundaries. Finally, the proposed dynamic model is a single variable transfer function that fails to capture the non-linearities of the system and does not take into account its parametric uncertainty.

The first contribution of this work is to propose a modular state-space multi-variable dynamic model of an m-terminal PFC, along with a generic grid model. It highlights the parametric uncertainties of the system, as well as its non-linearities. Based on this model, the second contribution is to establish a first multi-variable control law. It achieves simultaneous direct balancing control of the power in each line and voltage control of the reservoir capacitor. No additional hardware is required. Local properties of asymptotic stability and robustness of the resulting closed-loop are assessed on a tenth scale experimental setup.

The rest of this paper is outlined as follows. In the second section, the control problem is stated, the dynamical equations of the system are provided adopting a state-space formulation. The third section is devoted to the design of the control law. An integral action is first added. Then, the bilinear dynamics are analytically linearised to compute the control gain matrices through eigenvalue assignment. The fourth section focuses on experimental results, before giving concluding remarks in the last section.

Notations. The symbol $\mathbf{I}_m$ stands for the identity matrix of size $m \times m$. The null matrix of size $m \times n$ is denoted by $\mathbf{0}_{m\times n}$ while $\mathbf{0}_m$ denotes a column vector. Dimensions are omitted when it is obvious from the context. The operator "diag$\{\}$" builds a diagonal matrix from entries of the input vector argument. Finally, given vector a, the notation a_k refers to the k-th element of a, with 1 being the index of first element.

Problem statement and modelling

Problem statement and control objectives

The objective of this study is to achieve power control in the line connected to each terminal of the PFC while maintaining the reservoir voltage to a fixed value, despite the uncertainty of the grid. This reservoir voltage is constant if and only if the sum of powers in each line equals zero. Consequently, if the lines numbered k from one to $m-1$ are regulated to their corresponding **constant line power reference $\mathbf{P}^{\mathbf{r}}_{\mathbf{k}}$**

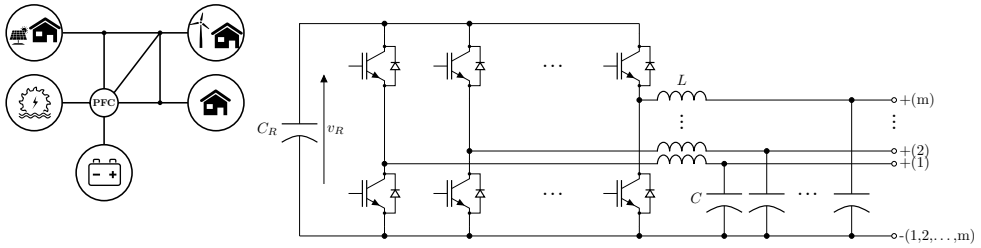

(a) Micro-grid example with a 5-terminal PFC

(b) m-terminal DC Power Flow Controller

Fig. 1: Studied converter in its context

and the reservoir capacitor is regulated to its **constant reservoir voltage reference $\mathbf{v_R^r}$**, the power in the unregulated line (here, line m) will naturally converge to the overall power balance ($P_m \to -\sum_{k=1}^{m-1} P_k^r$).

To maintain flexibility and modularity, the control law should be designed for a set of possible micro-grids. Limited knowledge should be assumed on their model, so that the dynamics of each branch is partially unknown from the PFC viewpoint.

The problem tackled in this paper is the following: Given line power references P_k^r, ($k \in \{1,\dots,m-1\}$) and a reservoir voltage reference v_R^r, design a feedback controller delivering the gate voltages of IGBTs such that the power flowing though the k-th line and the reservoir voltage asymptotically converge respectively to P_k^r and v_R^r, despite uncertainties on each line. This study does not tackle the problem of defining P_k^r and v_R^r. They are assumed to be given and reachable.

System dynamic model

In this section, a dynamic model for an m-terminal PFC is proposed.

The grid as seen by the k-th terminal is modelled as the series connection of an inductance, a resistor and a constant voltage source. In this case, the electrical model related to the k-th branch of the PFC and the proposed grid model as seen by this terminal are depicted on Fig. 2. Let us emphasize that different L_{Gk}, R_{Gk} and V_{Gk} can be considered for each terminal.

Some parameters in the model are considered unknown or uncertain to take into account the high variability of the grid: V_{Gk}, R_{Gk} and L_{Gk} ($k \in \{1,\dots,m\}$). They are, however, considered bounded between a known max and min values. The other parameters (L, C and C_R) depend on the design of the converter and are therefore known.

An averaged model over a switching period is introduced. The PWM duty cycle (ratio) of the k-th branch is noted d_k. The averaged voltages and currents are noted on Fig. 2. The dynamic equations read, with $k \in \{1,\dots,m\}$:

$$\frac{dv_R}{dt} = \frac{1}{C_R}\sum_{k=1}^{m} i_k d_k, \tag{1a}$$

$$\frac{di_k}{dt} = \frac{1}{L}(v_k - v_R d_k), \tag{1b}$$

$$\frac{dv_k}{dt} = \frac{1}{C}(i_{Gk} - i_k), \tag{1c}$$

$$\frac{di_{Gk}}{dt} = \frac{1}{L_{Gk}}(V_{Gk} - R_{Gk} i_{Gk} - v_k) \tag{1d}$$

$$P_k = i_{Gk} v_k. \tag{1e}$$

Remark 1. In the case where another PFC is connected at the end of the line, it is assumed it controls the voltage instead of the power, and can therefore be modelled as a voltage source: take R_{Gk} as the line resistance and V_{Gk} as the nominal line voltage. ⌟

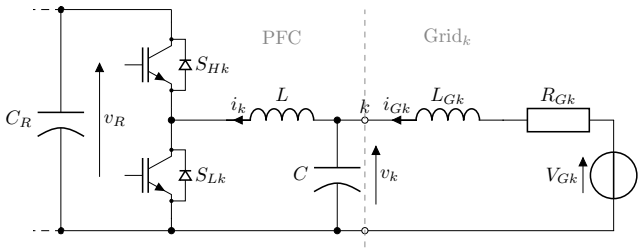

Fig. 2: Detail of k-th branch of the PFC (left) and the proposed grid model as seen by this terminal (right)

State-space model

To account for the coupling between the dynamics of the branches induced by C_R, a multivariable viewpoint is adopted. Recall that the vector notation of any element a_k is $a = [a_1, a_2, \dots]^\intercal$. The input vector is then made of the duty cycles $u = d$, the state vector gathers the voltage across all capacitors and the current in all inductors $x = [v_R, i^\intercal, v^\intercal, i_G^\intercal]^\intercal = [v_R, i_1, \dots, i_m, v_1, \dots, v_m, i_{G1}, \dots, i_{Gm}]^\intercal$ and the output vector corresponds to the following controlled variables $y = [P_1, \dots, P_{m-1}, v_R]^\intercal$. All the uncertain parameters are gathered in a vector $\theta = [L_G^\intercal, R_G^\intercal, V_G^\intercal]^\intercal = [L_{G1}, \dots, L_{Gm}, R_{G1}, \dots, R_{Gm}, V_{G1}, \dots, V_{Gm}]^\intercal$.

This allows to rewrite (1) under the state-space form:

$$\begin{cases} \dot{x}(t) = f(x(t), u(t)) = A(\theta)x(t) + N(x(t))u(t) + q(\theta) \\ y(t) = h(x(t)) \end{cases}, \tag{2a}$$

with

$$J(\theta) = \operatorname{diag}\{C_R, L, \dots, L, C, \dots, C, L_{G1}, \dots, L_{Gm}\}, \tag{2b}$$

$$A(\theta) = J(\theta)^{-1} \begin{bmatrix} 0 & \mathbf{0}_m^\intercal & \mathbf{0}_m^\intercal & \mathbf{0}_m^\intercal \\ \mathbf{0}_m & \mathbf{0} & \mathbf{I}_m & \mathbf{0} \\ \mathbf{0}_m & -\mathbf{I}_m & \mathbf{0} & \mathbf{I}_m \\ \mathbf{0}_m & \mathbf{0} & -\mathbf{I}_m & \operatorname{diag}\{-R_G\} \end{bmatrix}, \tag{2c}$$

$$N(x) = J(\theta)^{-1} \begin{bmatrix} i^\intercal \\ -v_R \mathbf{I}_m \\ \mathbf{0}_{2m \times m} \end{bmatrix}, \tag{2d}$$

$$q(\theta) = J(\theta)^{-1} [\mathbf{0}_{2m+1}, V_G^\intercal]^\intercal, \qquad h(x) = [i_{G1} v_1, \dots, i_{Gm-1} v_{m-1}, v_R]^\intercal. \tag{2e}$$

This system is bilinear and uncertain with a non-linear (quadratic) output, making the control design very challenging.

Proposed control method

For simplicity, the design of the control law is presented here for a 3-terminal PFC, i.e. $m = 3$.

Multi-variable PI controller

Since there are uncertain parameters in the model, the equilibrium point to reach is also uncertain. This means that a simple state feedback control would lead to steady-state errors in the event of a change in the grid model. To cancel this deviation, an integral action is added to make sure the control objectives are asymptotically reached. Thus, a multi-variable proportional integral control law is proposed:

$$\dot{z}(t) = h(x(t)) - r, \tag{3a}$$

$$u(t) = K_p x(t) + K_i z(t) + u_{ff}, \tag{3b}$$

where $r = [P_1^r \; P_2^r \; v_R^r]^\intercal$ is the vector of reference values and u_{ff} is a constant feed-forward term. Recall that $h(x(t)) = [P_1(t) \; P_2(t) \; v_R(t)]^\intercal$. The rest of this section is devoted to the computation of the controller

parameters $K_p \in \mathbb{R}^{m\times(3m+1)}$, $K_i \in \mathbb{R}^{m\times m}$ and $u_{ff} \in \mathbb{R}^m$.

Linearised (small-signal) augmented model

Let us append the states z (integrator of (3a)) to x, creating an augmented state vector $x_a = [x^\intercal, z^\intercal]^\intercal$. The augmented dynamics $\dot{x}_a = f_a(x_a, u)$ read:

$$f_a\left(\begin{bmatrix} x \\ z \end{bmatrix}, u\right) = \begin{bmatrix} f(x,u) \\ h(x) - r \end{bmatrix}. \tag{4}$$

Define $(x_a^\star, u^\star)$ as a constant pair zeroing the derivative of x_a, i.e. $f_a(x_a^\star, u^\star) = 0$. The entries of $(x_a^\star, u^\star)$ are identified via the superscript *. From (1) and (3a), one gets the following equilibrium:

$$v_R^\star = v_R^r, \tag{5a}$$

$$u_k^\star = \frac{V_{Gk} + \sqrt{V_{Gk}^2 - 4P_k^r R_{Gk}}}{2v_R^r}, \tag{5b}$$

$$v_k^\star = u_k^\star v_R^r, \tag{5c}$$

$$i_{Gk}^\star = \frac{P_k^r}{v_k^\star}, \tag{5d}$$

$$i_k^\star = i_{Gk}^\star, \tag{5e}$$

with $k \in \{1, \ldots, m\}$ and $P_3^r := -P_1^r - P_2^r$. Let us select $z^\star = 0$ since this vector can be defined arbitrarily. Observe that $u^\star$ and, in turn $x_a^\star$, depend on the unknown model parameters V_{Gk} and R_{Gk} (the entries of θ), and also on the reference values P_k^r and v_R^r (the entries of r).

Let us now linearise the augmented model (4) at the equilibrium $(x_a^\star, u^\star)$. One gets

$$\dot{\tilde{x}}_a = A_a(\theta, r)\tilde{x}_a + B_a(\theta, r)\tilde{u}, \tag{6a}$$

where $\tilde{x}_a = x_a - x_a^\star$ and $\tilde{u} = u - u^\star$ are respectively the state and input in relative coordinates, and

$$J_a(\theta) = \operatorname{diag}\{J(\theta), \mathbf{I}_3\}, \qquad B_a(\theta, r) = J_a(\theta)^{-1}\begin{bmatrix} i^{\star\intercal} \\ -v_R^r \mathbf{I}_3 \\ \mathbf{0}_{9\times 3} \end{bmatrix}, \tag{6b}$$

$$A_a(\theta, r) = J_a(\theta)^{-1}\begin{bmatrix} 0 & u^{\star\intercal} & \mathbf{0}_3^\intercal & \mathbf{0}_3^\intercal & \mathbf{0}_3^\intercal \\ -u^\star & \mathbf{0} & \mathbf{I}_3 & \mathbf{0} & \mathbf{0} \\ \mathbf{0}_3 & -\mathbf{I}_3 & \mathbf{0} & \mathbf{I}_3 & \mathbf{0} \\ \mathbf{0}_3 & \mathbf{0} & -\mathbf{I}_3 & \operatorname{diag}\{-R_G\} & \mathbf{0} \\ \begin{bmatrix} 0 \\ 0 \\ 1 \end{bmatrix} & \mathbf{0} & \operatorname{diag}\{i_{G1}^\star, i_{G2}^\star, 0\} & \operatorname{diag}\{v_1^\star, v_2^\star, 0\} & \mathbf{0} \end{bmatrix}. \tag{6c}$$

Computation of the controller parameters

The linearised system (6a) *at the nominal operating point* θ_n *and* r_n (see Table I for numerical values) can then be stabilized using the control law $\tilde{u} = K\tilde{x}$. The eigenvalues of $A_a(\theta_n, r_n) + B(\theta_n, r_n)K$ are assigned by choosing the appropriate gain K through pole placement. The target poles are here chosen as the spectrum of $A_a(\theta_n, r_n)$ except for the three eigenvalues at zero (due to the integral action) that are shifted on the left hand side of the complex plane.

Such a strategy leads to a controller ensuring local asymptotic stability under nominal reference and operating point, i.e. for $r = r_n$ and $\theta = \theta_n$. A continuity argument can be invoked to prove that such a property remains valid in a neighbourhood of (θ_n, r_n), i.e. the stability is preserved if the references and the uncertainties on the grid are slightly modified.

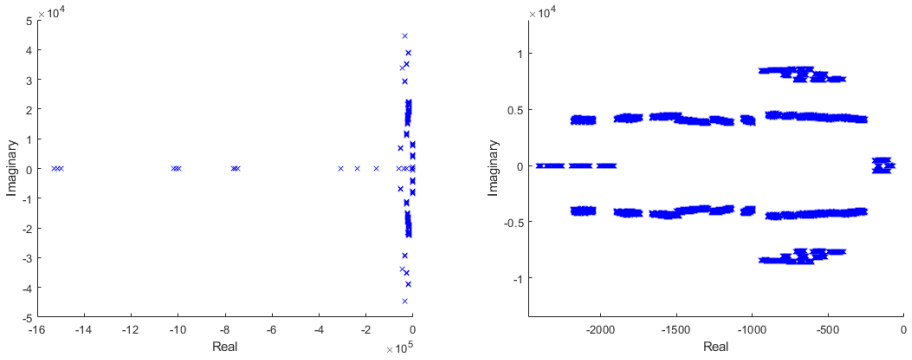

Fig. 3: Eigenvalues of $A_a(\theta_s, r_s) + B_a(\theta_s, r_s)K$ for each sample (θ_s, r_s), displayed with two levels of zoom

Table I: Operating conditions for the tenth scale setup

	Parameter	Value $k=1$	Value $k=2$	Value $k=3$	Unit		Parameter	Value	Unit
	L_{Gk}	18	18	18	µH		P_1^r	-50	W
θ_n	R_{Gk}	21.7	24.5	1.2	Ω	r_n	P_2^r	-50	W
	V_{Gk}	2	0	40	V		v_R^r	50	V
	L_{Gk}	18	18	18	µH		P_1^r	**-60**	W
θ_1	R_{Gk}	21.7	24.5	1.2	Ω	r_1	P_2^r	**-60**	W
	V_{Gk}	**10**	0	40	V		v_R^r	50	V

To estimate the degree of robustness of the closed-loop, the parameter domain in which θ and r belong to is sampled by successive increments on the different parameters (L_{Gk}, R_{Gk} or V_{Gk}). For each parameter, one sample is taken above the nominal value, and one is taken below, symmetrically. This results in three samples per parameter (nominal, higher and lower), and therefore in $3^9 = 19683$ tested parameter combinations. For each combination (θ_s, r_s), the location of the eigenvalues of $A_a(\theta_s, r_s) + B_a(\theta_s, r_s)K$ is depicted on Fig. 3. It comes out that every eigenvalue is located in the left hand side of the complex plane, which suggests that K has good robustness properties and justifies the experimental scenario proposed in the next section.

Now that the gain K has been found, the real input u (the duty cycles) can be defined by the following equation:

$$u(t) = K(x_a(t) - x_a^\star(\theta_n, r_n)) + u^\star(\theta_n, r_n), \tag{7}$$

which is equivalent to (3b), with K_p being the ten first columns of K and K_i the three last ones, and $u_{ff} = -Kx_a^\star(\theta_n, r_n) + u^\star(\theta_n, r_n)$.

Experimental results

The experimental setup is presented in Fig. 4 and 5. A dSPACE MicroLabBox (µLB) rapid prototyping system (a) is used to control the PFC (b). The first terminal of the PFC is connected to a voltage-controlled electronic load (EL) in series with a resistor (R) in (f), through 30 m of standard U1000 RV2 cable (Line_k) in (d). The second terminal is similarly connected to a resistor (e), and the third terminal to a power supply (PS) in (c). The switching devices used in the PFC are NGTB30N120LWG IGBTs. The numerical values of the components are listed in Table II. It includes the inductance and capacitance values as well as the parasitic resistances (series inductor resistance and parallel capacitor resistance), and the switching frequency and dead time of the PWM. The feedback state measurements are synchronised with the PWM and filtered with first-order filters of time constants T_f.

Table II: Converter parameters

Parameter	Value	Parameter	Value
L	760 µH	r_L	1 Ω
C	20 µF	r_C	4.3 mΩ
C_R	60 µF	r_{C_R}	10 mΩ
F_{SW}	15 kHz	$t_{dead-time}$	0.3 µs
T_f	1 ms		

Table III: Experimental scenario

t	0.17 s		0.67 s
θ	θ_n	θ_n	θ_1
r	r_n	r_1	r_1

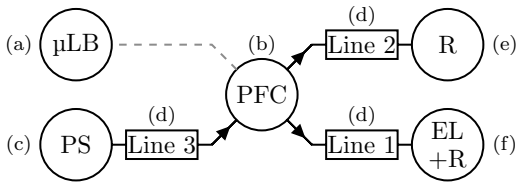

Fig. 4: Drawing of the experimental setup

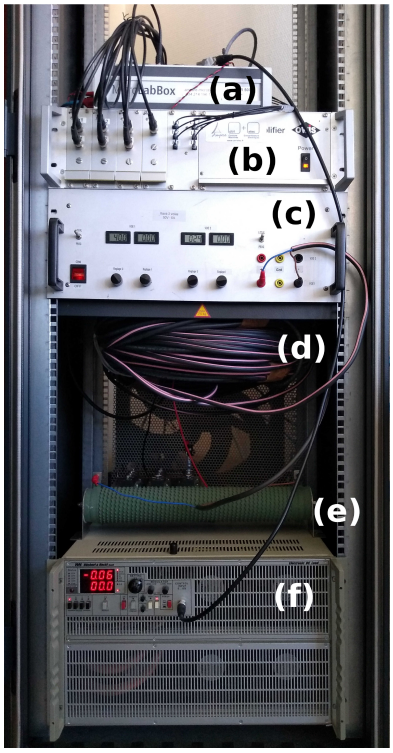

Fig. 5: Picture of the experimental setup

To validate the proposed non-linear model (2a), it is excited in simulation with steps in duty cycle, and the same is done on the experimental setup. The resulting signals are displayed on top of each other on Fig. 6. It appears clearly that this model accurately captures the system's dynamics but not its losses. Indeed the discrepancy between $P_{3,meas}$ and $P_{3,sim}$ is the power lost in the PFC. This large value (40 W) can be explained by the fact that the setup is currently used at 5% of its rated power. These losses will be modelled in future studies for a final validation of the control process, but the simplicity of the proposed model is necessary for the design of control methods. The next paragraph shows that the proposed controller can fully cope with these inaccuracies.

The proposed control law is tested experimentally at a tenth scale through different phases. During the first one, the references and operating point are initially at their nominal values, before being modified according to Table III and using the values from Table I. The change in θ corresponds to a step from 2 V to 10 V on the electronic load. The resulting reservoir voltage and line powers are displayed in Fig. 7, while the state variables and duty cycles are displayed in Fig. 8.

Observe on Fig. 7 that the change in power references for lines 1 and 2 leads to a spike on the reservoir voltage. Furthermore, observe on Fig. 8 that the control action is soft enough to prevent the saturation of the duty cycles. By speeding up the controller (choosing larger eigenvalues), one can reduce the voltage spike while decreasing the convergence time, although this will be done at a cost in robustness and may lead to the saturation of the duty cycles. On the bottom right figure, P_3^r is given as the theoretical value P_3 should reach in a lossless system, which explains the observed discrepancy. Although the change occurring at $t = 0.67$ s only is on line 3, it should be noted that it has a repercussion on all the other lines and on the reservoir voltage. This is due to the coupling of the lines, induced by the reservoir capacitor. Indeed, C_R has relatively small magnitude, 60 µF.

Conclusion

In this paper, a dynamic model of an m-terminal PFC is proposed by adopting a multi-variable viewpoint to account for the coupling in the dynamics. The uncertain nature of a micro-grid is also explicitly taken into account, so that the unknown parameters appear in the model.

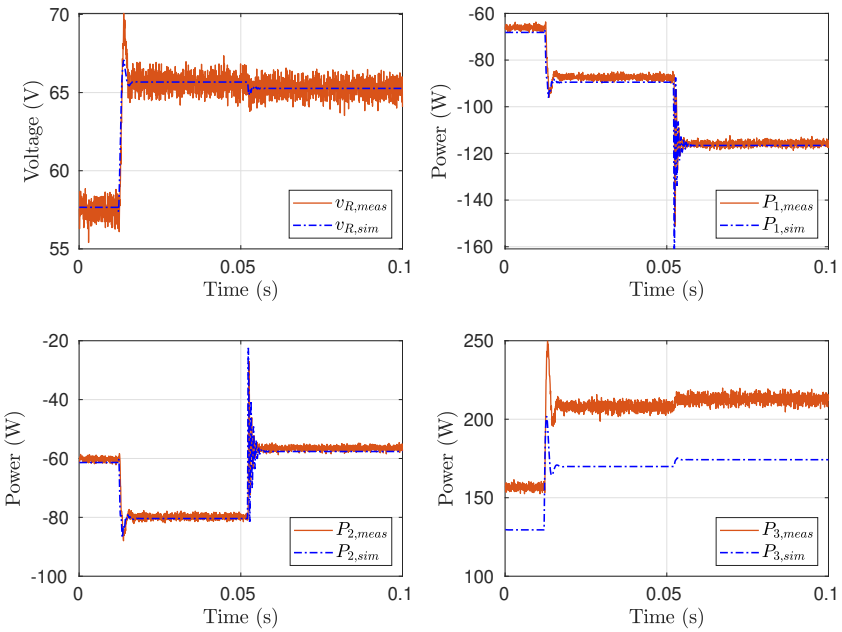

Fig. 6: Open-loop step response of the proposed model compared to the experimental setup (unfiltered measurements). The applied duty cycles are, for each phase, $[0.7, 0.7, 0.6]^\intercal$, $[0.7, 0.7, 0.5]^\intercal$, $[0.8, 0.6, 0.5]^\intercal$.

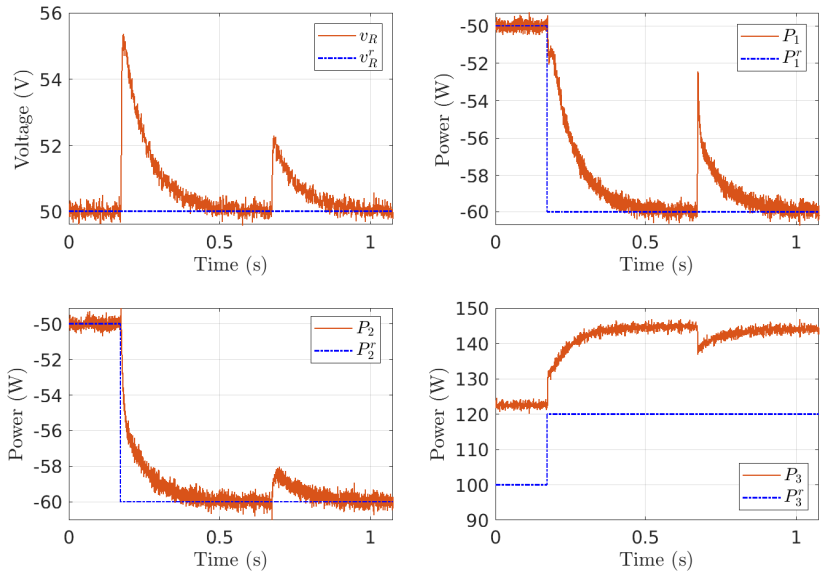

Fig. 7: Reservoir voltage and line power measurements on the experimental setup in closed-loop with the proposed controller, for a step in line power references followed by a step on the load voltage.

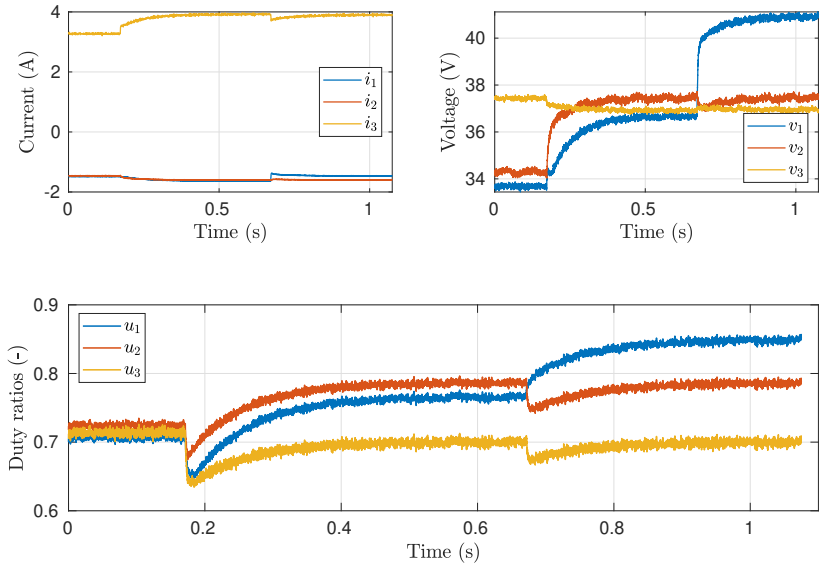

Fig. 8: Inductor currents, line voltages and duty cycle measurements on the experimental setup in closed-loop with the proposed controller, for a step in line power references followed by a step on the load voltage

Moreover, a feedback control law has been proposed, in the case of a three terminal PFC. Robust asymptotic properties have been achieved, locally in the state space and locally in the parametric space. Simultaneous control of the power in each line and of the reservoir voltage of the converter is achieved. Those results have been successfully validated on a tenth scale experimental setup, for different references and operating points.

Further studies will mainly follow two different paths. First, increase the robustness of the control law by taking uncertainties into account beforehand, that is at the controller gains computation step. Second, achieve global or regional stability by enlarging as much as possible the basin of attraction of the closed-loop system.

References

[1] D. Kumar, F. Zare, and A. Ghosh, "DC Microgrid Technology: System Architectures, AC Grid Interfaces, Grounding Schemes, Power Quality, Communication Networks, Applications, and Standardizations Aspects," en, *IEEE Access*, pp. 12 230–12 256, 2017.

[2] *Solar Powered Health Clinics in Peru Strengthen Community Resilience*, Sep. 2020.

[3] P. Vannini and J. Taggart, *Off the grid: re-assembling domestic life*, en, ser. Innovative ethnographies. New York: Routledge, 2015.

[4] S. Anand and B. G. Fernandes, "Optimal voltage level for DC microgrids," en, in *IECON 2010 - 36th Annual Conference on IEEE Industrial Electronics Society*, Glendale, AZ, USA: IEEE, Nov. 2010, pp. 3034–3039.

[5] A. T. Elsayed, A. A. Mohamed, and O. A. Mohammed, "DC microgrids and distribution systems: An overview," en, *Electric Power Systems Research*, pp. 407–417, Feb. 2015.

[6] E. Rodriguez-Diaz, J. C. Vasquez, and J. M. Guerrero, "Potential Energy Savings by Using Direct Current for Residential Applications: A Danish Household Study Case," en, p. 6, 2017.

[7] A. Ammous and H. Morel, "LVDC: An Efficient Energy Solution for On-Grid Photovoltaic Applications," en, *Smart Grid and Renewable Energy*, pp. 63–76, 2014.

[8] L. Mackay, "Toward the Universal DC Distribution System," en, pp. 1032–1042, Jul. 2017.

[9] S. Balasubramaniam, C. E. Ugalde-Loo, and J. Liang, "Series Current Flow Controllers for DC Grids," en, *IEEE Access*, pp. 14 779–14 790, 2019.

[10] D. Fregosi, S. Ravula, D. Brhlik, J. Saussele, S. Frank, E. Bonnema, J. Scheib, and E. Wilson, "A comparative study of DC and AC microgrids in commercial buildings across different climates and operating profiles," en, in *2015 IEEE First International Conference on DC Microgrids (ICDCM)*, Atlanta, GA, USA: IEEE, Jun. 2015, pp. 159–164.

[11] M. Barara, H. Morel, and G. Clerc, "Control Strategy Scheme for Consistent Power Flow Control in Meshed DC Micro-grids," en, 2017, pp. 1–10.

[12] Y. Takahashi, K. Natori, and Y. Sato, "A multi-terminal power flow control method for next-generation DC power network," en, in *2015 IEEE Energy Conversion Congress and Exposition (ECCE)*, Montreal, QC, Canada: IEEE, Sep. 2015, pp. 6223–6230.

[13] K. Natori, Y. Nakao, and Y. Sato, "A Novel Control Approach to Multi-Terminal Power Flow Controller for Next-Generation DC Power Network," in *2018 International Power Electronics Conference (IPEC-Niigata 2018 -ECCE Asia)*, May 2018, pp. 588–592.